International Deep Drawing Research Group
IDDRG 2009 International Conference
1-3 June 2009, Golden, CO, USA

FAILURE ANALYSIS OF ADVANCED HIGH STRENGTH STEELS (AHSS) DURING DRAW BENDING

Hyunok Kim[1], Alexander R. Bandar[2], Yu-Ping Yang[1], Ji Hyun Sung[3], and R.H. Wagoner[3]

[1] Edison Welding Institute (EWI)
1250 Arthur E. Adams Drive, Columbus, Ohio 43221-3585
e-mail: hkim@ewi.org, Webpage: www.ewi.org

[2] Scientific Forming Technologies Corporation (SFTC)
2545 Farmers Drive, Suite 200
Columbus, Ohio 43235
e-mail: abandar@deform.com, Webpage: http://www.deform.com

[3] Department of Materials Science and Engineering
The Ohio State University
2041 College Road, Columbus, OH 43210-1124
e-mail: wagoner@matsceng.ohio-state.edu, Webpage: http://www.matsceng.ohio-state.edu/cammac

ABSTRACT

Advanced High Strength Steels (AHSS) have been increasingly used for body structures by the automotive industry for better crash worthiness and fuel economy. However, manufacturing automotive structural components with AHSS poses new forming challenges. One of these challenges is shear fracture that more often occurs when AHSS material is drawn and bent at the radius of forming tools.

In this study, shear fractured samples of various automotive AHSS structure components (B-pillar and side rail parts) were examined to investigate the fracture mode (i.e. ductile or brittle) by SEM (Scanning Electron Microscope). It was found that most of the shear fractured samples exhibited ductile dimpled structures by micro-void coalescence. To further understand the microvoid formation and growth at different plastic strains, several stop-tensile tests were conducted between the ultimate tensile strength and the final failure for DP590 material. Micrographs were taken to quantify the void formation and growth in the necking area of these tensile specimens. As plastic strain increased during the test, the presence of micro-voids and microcracks considerably increased after necking, particularly for elongations close to the failure point. This suggests that micro-damage in the form of voids accumulates until final failure. To investigate whether practical formability under bending and drawing conditions can be predicted using industry-standard techniques, tensile tests were FE simulated isothermally up to failure using tensile stress-strain laws extrapolated from measured tensile stress-strain curves. The Cockcroft-Latham damage accumulation model was introduced in the simulations, with the result that the failure elongations were not predicted properly. A critical damage value (CDV) was then determined to minimize the error in simulated and measured tensile elongations. The CDV established in tension was used with isothermal FE simulation of draw-bend test results for various bend radii and draw speeds. This study demonstrated good agreements between the predicted failure modes and the experimental results. However, this energy-based damage model

underestimated the final drawing displacement at fracture compared to experiments. Therefore, it was concluded that a stress-strain-energy-based damage model should be improved for better FE predictions of shear fractures by considering the area fractions of micro-voids and thermal softening during deformation. In this study, the dual phase (martensite and ferrite) microstructure of DP590 was modeled and simulated to understand the micro-scale damage initiation and growth by using commercial FEM code, DEFORM.

Keywords: Stamping: Shear Fracture; Finite Element Method (FEM); Advanced High Strength Steels (AHSS).

1. INTRODUCTION

Shear fracture has been observed during stamping of AHSS, without appreciable thinning before fracture. From the literature review, such shear cracking was not typically encountered in traditional HSLA steels during forming. Moreover, this type of early fracture cannot be predicted by using a conventional Forming Limit Diagram (FLD) of AHSS.

While HSLA has only ferrite and pearlite microstructures in the sheet, most AHSS have multi-phase microstructures such as ferrite, bainite, martensite, and retained austenite. Therefore, the response of inhomogeneous microstructures in AHSS should be considered as one of the important sources of the unusual shear fracture behavior that is not experienced in HSLA or low carbon steels. The complexity of the microstructure may cause a shear-localization mode that involves little macroscopic necking under particular forming condition such as bending.

The heterogeneity in microstructure of AHSS leads to non-uniform deformation among the phases. The interaction between the phases can cause stress concentration and strain partition [1]. During the rolling process of the dual phase steel, micro-scale cracks can be induced in the sheet surface with martensitic islands. Under subsequent forming conditions, these small cracks can grow and lead to early fracture. It is well known that the strength and crack resistance of multi-phase microstructure steels depends on their morphology, distribution, and hardening of individual microstructures [2, 3, 4, 5]. The apparent shear failure shows some characteristics of the transition from ductile to brittle failure. While the crack initiation may be ductile, its propagation can change to brittle under certain loading conditions [6]. These findings show that microstructure plays an important role in the fracture properties of material.

In sheet forming processes, the FLD has been conventionally adopted for evaluating failure based on necking and ductility. Most theoretical studies on the FLD have been based on the localized necking approach developed by Marciniak and Kuczynski [7]. In this approach, the existence of material imperfections is assumed to lead the unstable growth of strain in the weaker regions due to the presence of inhomogeneities in load bearing capacity, and subsequently produces localized necking and failure. A primary drawback of strain based FLDs is that they are valid only during proportional loading [8,9]. That is because the constitutive equations governing the stress-strain relations are path-dependent [10]. During metal stamping process, the state of stress and strain in the part changes continuously and varies at different locations of part.

A practical criterion for predicting shear fracture behavior is not currently available. Therefore, a new failure criterion needs to be developed to predict shear cracking so that product and tooling design can be performed correctly to avoid shear fracture during stamping. The study addressed in this paper covers i) the feasibility study of FEM with existing energy based damage model for predicting shear fractures observed in draw-bending AHSS, and ii) the effects of

growth/coalescence of micro-voids on material failure by using the stop-tensile test and numerical simulations.

2. EXAMINATIONS OF SHEAR FRACTURE PARTS

2.1 Visual inspections

Shear fractured auto body structure components such as B-pillar and Rail parts were qualitatively examined. DP980 showed severe cracking in the draw bead areas as shown in Figure 1. In a stamping rail part using DP600, shear cracking was observed in a near plane-strain bending area as shown in Figure 2.

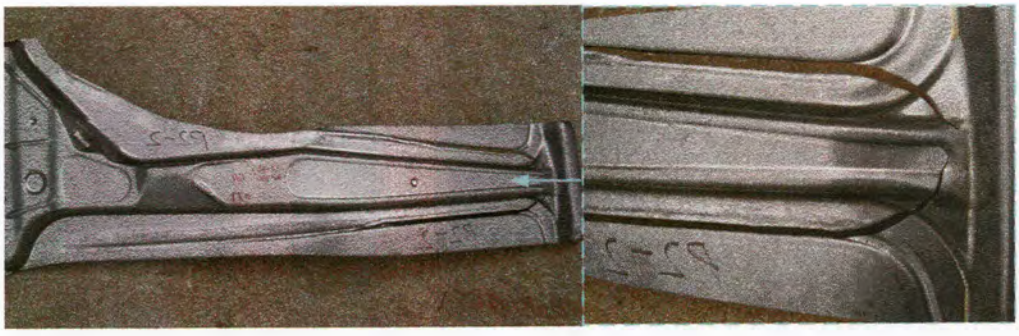

Figure 1. *Shear fracture observed in B-pillar part of DP980*

Through visual inspections of production parts, shear fractures were more often experienced in the following areas:

- Bending area at the smaller bending radius (i.e. small R/t ratio)
- Stretch-bending area at draw-beads (i.e. moderate R/t ratio with stretching)
- Plane-strain bending area

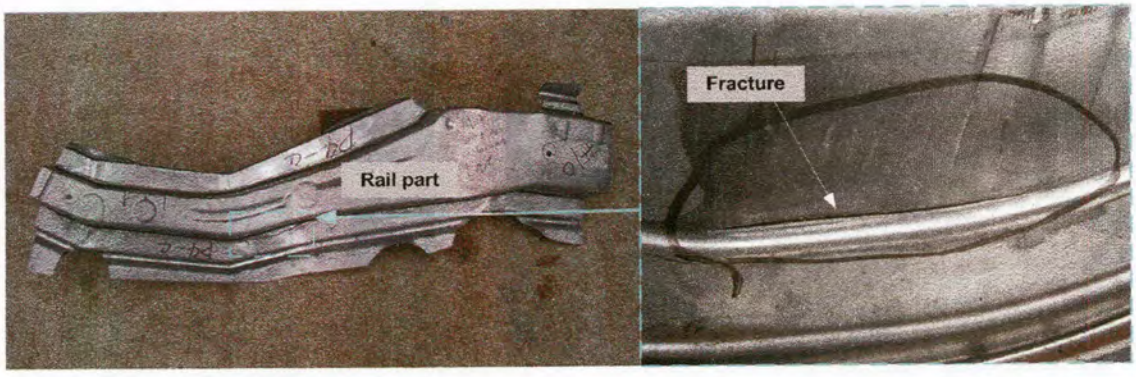

Figure 2. *Shear failure observed in Rail part of DP600*

2.2 SEM analyses

To understand the fracture mode, either brittle or ductile, the fractured B-pillar part and the laboratory tested draw-bend fractured specimen were examined using the SEM (Scanning Electron Microscope) as shown in Figures 3 and 4.

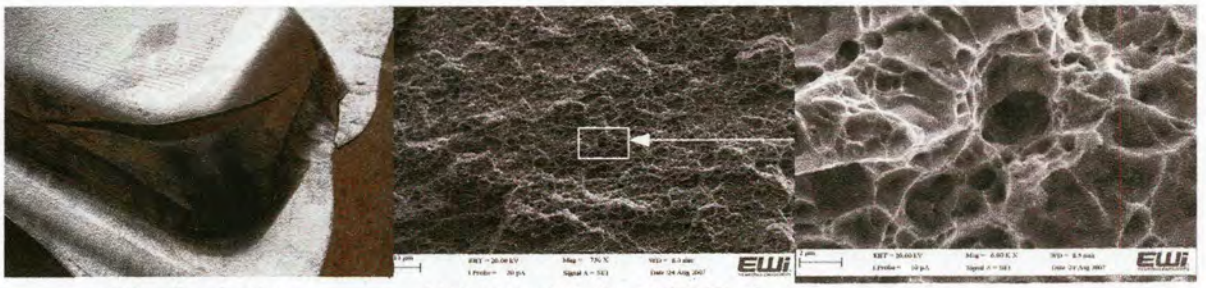

a) Bending fracture b) Fractured section (x750 Mag.) c) Porous structure (x1000 Mag.)

***Figure 3**. SEM results of failure in stretch bending area of B-pillar part (DP980)*

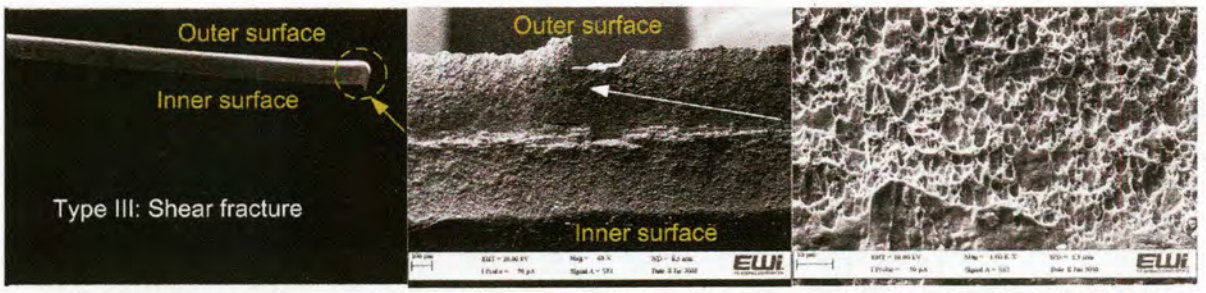

a) Shear fractured sample in draw bending test b) Cross section of fractured draw-bent sample (x60 Mag.) c) Fractured section (x1000 Mag.)

***Figure 4**. Draw-bend sample (DP590) and SEM results of fractured cross section*

SEM images of a fractured B-pillar part showed dimpled structures with a number of pores as shown in Figure 3. The shear fractured specimen tested with laboratory-scaled draw bend test also showed dimpled structure with many pores at the cross-section on fractured surface. It was found that fracture initiated in the middle of width, not from edges. The pores are a result of micro-void nucleation and coalescence. Although both fractured surfaces showed similar ductile dimple rupture, the draw bend sample showed more directionality of dimples toward the shear loading direction. Fractured sections of AHSS parts showed significant numbers of micro-voids. This finding indicates that the number and size of micro-voids increase as the plastic strain increases until fracture occurs. The stop-tensile test was used to monitor the growth and coalescence of micro-voids as the plastic stain increased [11].

3. STOP-TENSILE TESTS

3.1 Material

Dual Phase (DP) 590 material was used for this study. This material was supplied with no coating and its thickness was 1.4 mm. The detailed mechanical properties and chemical

compositions of this material are given in Table 1. A standard tensile test with 5 mm/min. crosshead speed at room temperature and its characterization methods (ASTM E8-04, ASTM E646-07, and ASTM E517-00) were used to obtain the mechanical properties such as yield strength (YS) and ultimate tensile strength (UTS).

Table 1. *Mechanical properties and chemical composition of DP590 steel in weight percent*

	Thickness (mm)			0.2% YS (MPa)		UTS (MPa)		e_u (%)		e_t (%)	n-value*		r-value	
	1.4			369		624		15.4		24.7	0.20		0.84	
DP590	C	Mn	P	S	Si	Cr	Al	Ni	Mo	Nb	Ti	V	B	
	0.08	0.85	0.009	0.007	0.28	0.01	0.02	0.01	<.01	<.002	<.002	<.002	<.0002	

* Chemical composition was analyzed at the GMNA Materials Laboratory (ASTM E415-99a)

3.2 Test results

The stop-tensile test was conducted to quantify the growth and coalescence of micro-voids as the plastic stain increased as shown in Figure 5. Six different points were used to stop the tensile loading from UTS to the final failure point (i.e. 14% stress drop from UTS). The measured engineering stress-strain curves to different stops are given in Figure 5. The cross-section areas of the tested specimens, both initially and at the stop point, are also listed there.

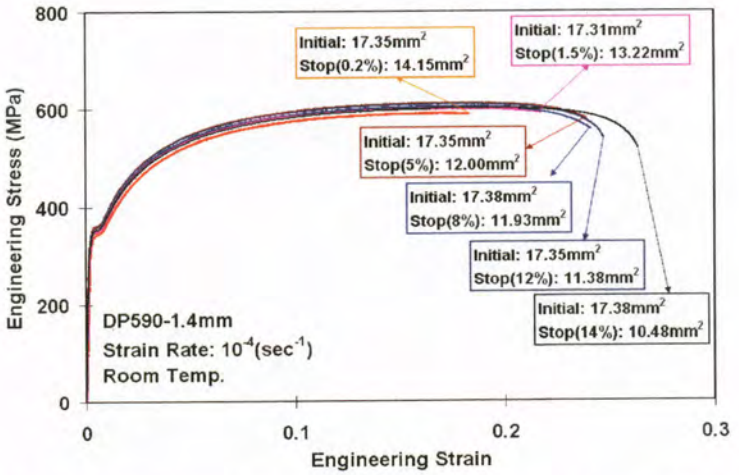

Figure 5. *Engineering stress-strain curves obtained in stop-tensile tests of DP590*

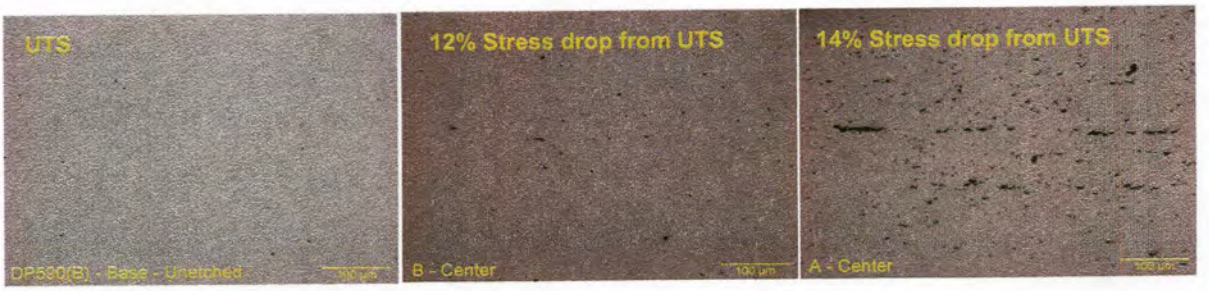

Figure 6. *Increase of micro-voids from UTS to failure*

The micrographs of samples taken from the necking or failed areas were further examined as shown in Figure 6. As the plastic stain increased, especially, close to the final failure point, the micro-voids showed significant growth and coalescence.

3.3 Characterization of micro-void formation

The area fraction of micro-voids of each micrograph (Figure 6) was calculated by using a commercial image processing and analysis software, Image-J. The area fraction of micro-voids is plotted with engineering stress and strain, respectively, in Figure 7.

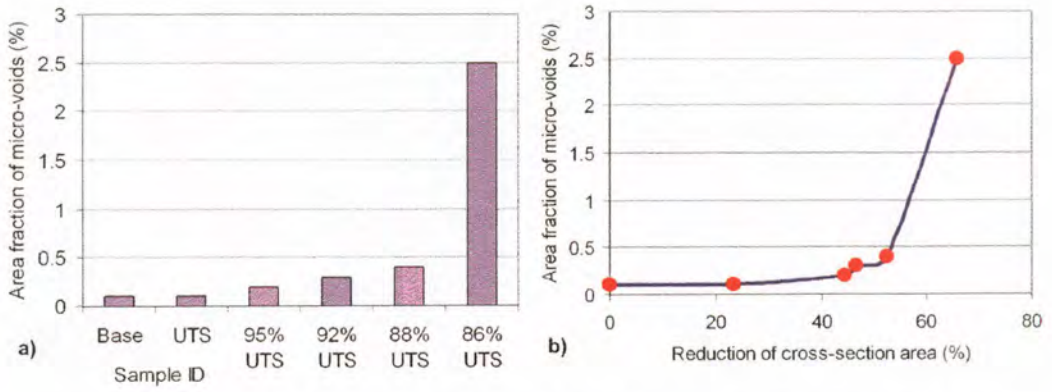

Figure 7. *The area fractions of micro-voids with respect to (a) stress and (b) strain*

As shown in Figure 7, the area fraction of micro-voids monotonically increased up to 88% UTS (i.e. 12% stress drop from UTS) and showed a very sharp increase of micro-voids near the failure point (i.e. 86% UTS). These results can indicate the following conclusions:

- The increase of micro-voids was not proportional to the plastic strain and stress value during plastic deformations.
- When the area fraction of micro-voids reaches a critical value that may be different for different materials, or the plastic stress and strain reach critical values, the material damage can be initiated and significantly accelerated in a non-linear behavior until the final fraction occurs.
- The rate of increase of micro-voids may vary for different loading conditions, for instances, uni-axial tension and draw-bending. However, the stress-strain energy that induces the damage of microstructure may not be significantly different regardless of loading path.
- With this assumption, the stress-strain based energy variable such as damage value can be tried for prediction of the shear fracture behavior in numerical modeling.

4. DETERMINATION OF CRITICAL DAMAGE VALUE (CDV)

To emulate the increase of micro-voids as the plastic stain increases, a damage model was used in FE simulations. Figure 8 shows a flow chart to determine the critical damage value (CDV) for sheet material.

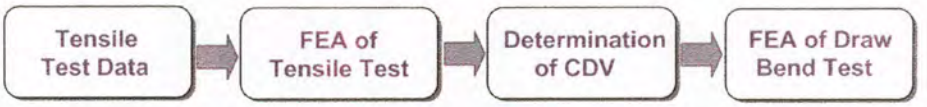

***Figure 8**. Flow chart for determining CDV*

A quarter 3-D FE model was prepared for tensile simulations and the distribution of damage value was plotted as shown in Figure 9-a. The material property of DP590 was obtained from the ASTM tensile test (ASTM E8-04). The true stress-strain data, as shown in Figure 9, was input to FE model. The measured data was used up to UTS and, after UTS the flow stress was extrapolated by using the Holloman's power law model as shown in Figure 9-b. The flow stress was assumed to be independent of strain-rate induced hardening and thermal-induced softening.

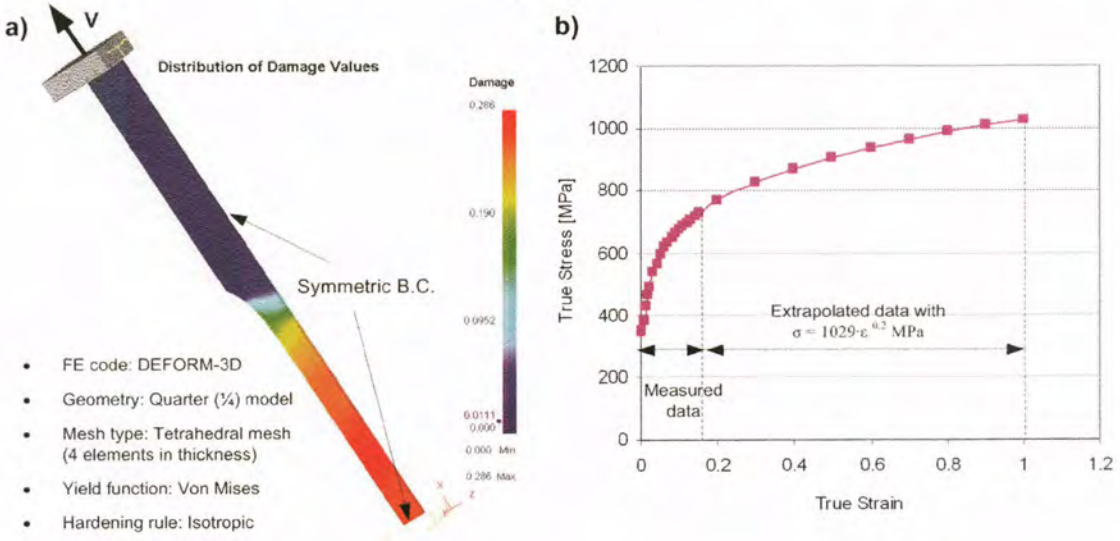

***Figure 9**. FE model (left) and true stress-strain data of DP590 tensile simulation (right)*

The Cockcroft & Latham damage model was adopted from among various damage models available in a commercial FEM code (DEFORM-3D), because this model showed a superior prediction of ductile fracture compared to other damage models in stamping Al materials [12]. More definitively, a "damage" parameter, proportional to the accumulated energy necessary to induce fracture can be used to determine a forming limit. Damage value, C, is defined as the integrated area beneath the stress-strain curve up to fracture as shown in Equation (1).

$$\int_0^{\bar{\varepsilon}_f} \frac{\sigma^*}{\bar{\sigma}} d\bar{\varepsilon} = C \qquad (1)$$

Where $\bar{\varepsilon}_f$ = fracture strain, $\bar{\varepsilon}$ = effective strain, $\bar{\sigma}$ = effective stress,

σ^* = maximum principal stress, C = damage value

From initial FE simulation without the critical damage value (CDV), the stress-strain energy as described in Equation (1) was calculated for tensile loading. The smaller CDV indicates the

earlier initiation of damage. The final CDV was determined as 0.35 by calibrating CDV to fit the stress-drop point with experiment as shown in Figure 10.

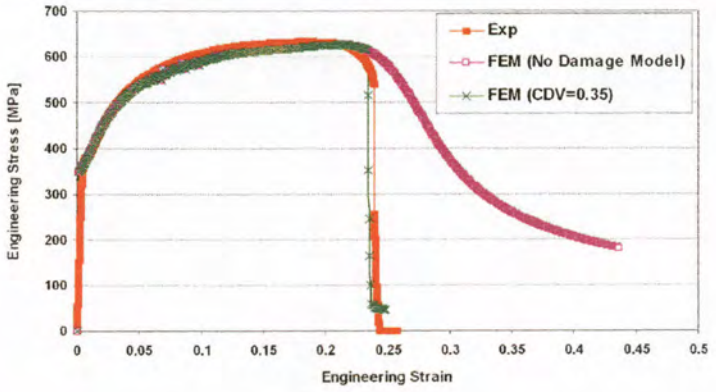

***Figure 10**. Comparison of engineering stress-strain data (DP590) between experiment and FE results*

5. VERIFICATION OF DAMAGE MODEL WITH DRAW BENDING TEST

The CDV determined from tensile test was verified by conducting FE simulations for draw bending tests at various conditions.

5.1 Draw bend test results of DP590

In the draw bending test, initially the specimen was 1.4 mm thick, 25.4 mm wide and 560 mm long. This specimen was initially bent with a roller and subsequently drawn with two grips holding both ends of the specimen as shown in Figure 11.

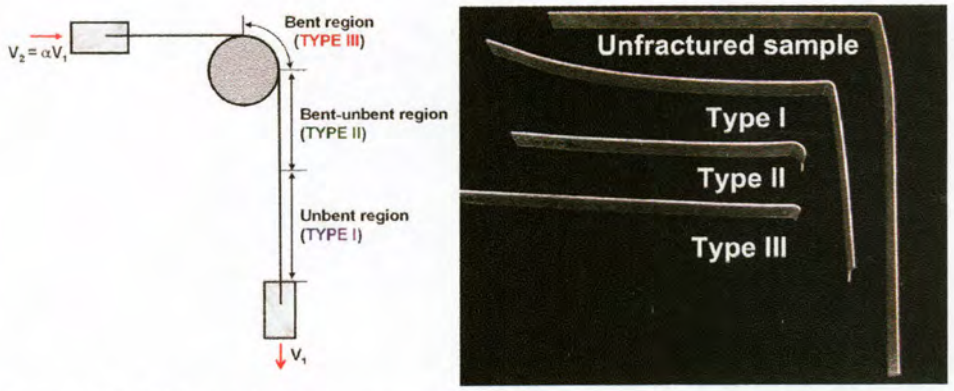

***Figure 11**. OSU-Draw bending test and the tested samples with various fracture types*

The velocities of the front and rear grips were controlled to be almost constant by a feedback control of hydraulic actuators to adjust the change of reactions during stretch-bending of the specimen. Five different R/t ratios (i.e. radius/thickness); 2.3, 3.4, 4.5, 7.9, and 13.6; were used with two different velocity ratios of front and rear grips (i.e. V2/V1). Depending on the R/t ratio and the velocity ratio, DP590 material showed three different fracture locations, namely, Type I, II and III as shown in Figure 11. While Type I was understood as tensile failure, Types II and III were categorized as shear failure during bending.

5.2 Draw bending simulation results

A FE model with mirror symmetry at half width was prepared to simulate the draw bending test as shown in Figure 12-a. The workpiece was assumed to be an elasto-plastic object and brick mesh was used with five elements in width and four elements in thickness. Different mesh density was used to improve the efficiency of computation and solution accuracy near the bending zone. With laboratory tests and modeling results at OSU, two different values of friction coefficient (μ=0.03 and 0.08) were recommended to use in FEA for V2=0 with a fixed roller and V2=13 mm/sec with a free roller. The same flow stress data (Figure 9-b) was used in draw bending simulations. FE simulations with the damage model successfully demonstrated different failure types as observed in experiments. Figure 12-b/c/d compares different failure types predicted by FEA with the damage model.

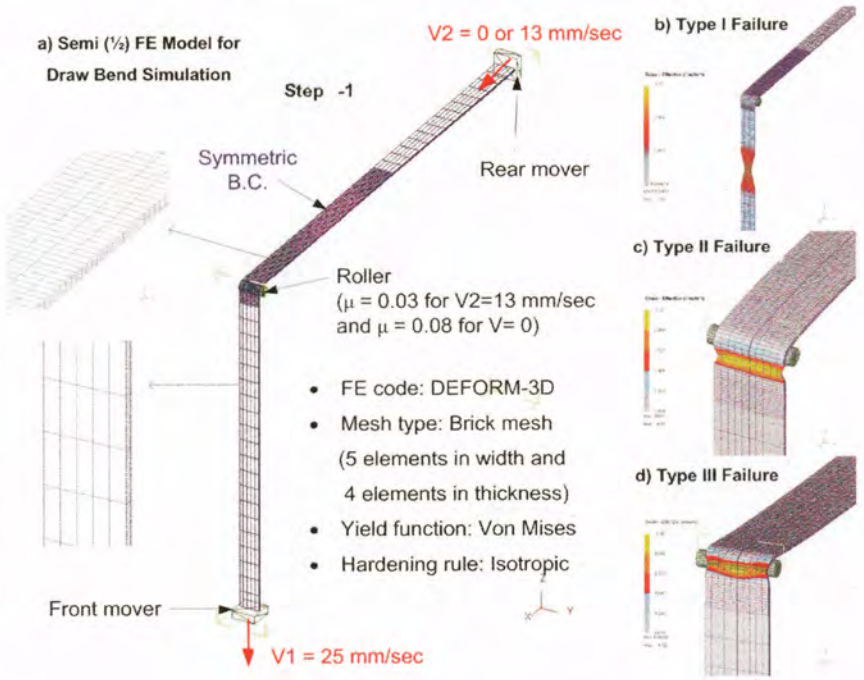

***Figure 12**. FE model for draw-bend test and predictions of different failure types*

In addition, FE simulations without the damage model were also conducted and their predictions of failure type and the final drawing displacement at fracture were compared with experiments and FEM with the damage model. As shown in Figure 13, both FE models showed good agreement with experimental results up to 20 mm displacement. However, in comparison to the experiment, FEM without damage model overestimated the load drop point compared to experiment, while FEM with the damage model slightly underestimated the load-drop point. The fracture point is indicated by the load-drop in Figure 13.

In comparison of failure type for the draw bending condition (i.e. V2=13 mm/sec and V1=25 mm/sec), Figure 14-a, FEM with the damage model showed good agreement with experiments while FEM without the damage model gave only tensile failure (Type-I) predictions, regardless of R/t ratio. Without the damage model, the FE-simulated load did not drop to zero, so the maximum thinning larger than 25% was regarded as the failure of material.

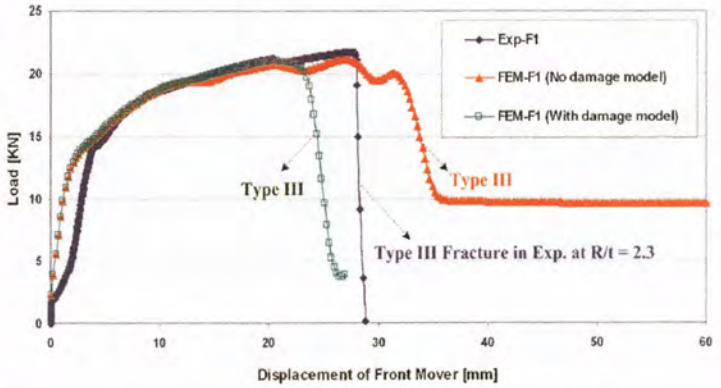

Figure 13. *Load-displacement curves of front grip for FE results and experiment (V1=25 mm/s and V2=0)*

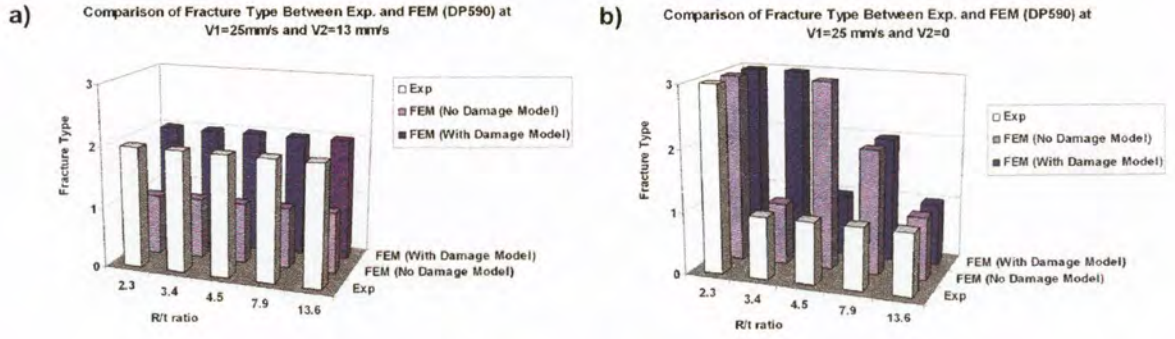

Figure 14. *Comparison of fracture type between Exp. and FEM*

In comparison of failure type at stretch bending condition (i.e. V2=0 and V1=25 mm/sec), Figure 14-b, FEM with the damage model showed good agreements with experiments at three R/t ratios: 2.3, 4.5, and 13.6. However, for R/t ratios of 3.4 and 7.9, FEM showed some discrepancies of failure type with experiments as shown in Figure 14-b.

6. NUMERICAL MODELING OF VOID FORMATIONS DURING TENSION

Preliminary numerical modeling for actual dual phase microstructure was attempted to simulate the growth of micro-voids at the boundary of martensite and ferrite phases. The original micrograph of DP590 was digitized by using the Scion image analysis program. The scanned edges were then imported and meshed into DEFORM for conducting numerical simulations. The flow stress of ferrite was referred from DEFORM material library. The flow stress of martensite was interpolated from the flow stress of DP590 obtained with a macro tensile test and the referred flow stress of ferrite as shown in Figure 15. The measured volume fraction of martensite and ferrite was considered to interpolate the flow stress of martensite. Thermal softening behavior for each phase was also considered in the simulation by extrapolating the comparative behaviors of the ferrite and martensite in the DEFORM material library. The Representative Volume Element (RVE) selected for these simulations included approximately 17% martensite and 83% ferrite.

Figure 16 shows the evolution of microvoids between martensite and ferrite phases as the strain increases. The numerical model was able to run only up to strain 0.05, because of the difficulty of converging numerical solutions. Therefore, numerical modeling of realistic microstructure may not be practical and efficient to predict the growth of micro-voids and linkage into a macro scale fracture in the large plastic stain range for sheet metal forming.

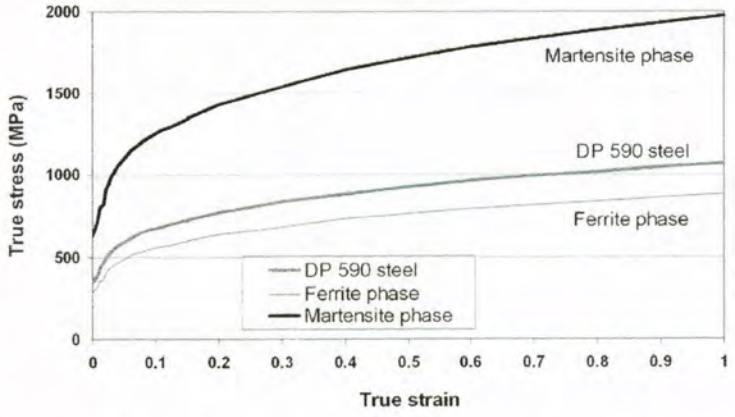

Figure 15. *Flow stress behaviors of DP590/ ferrite/ martensite versus strain.*

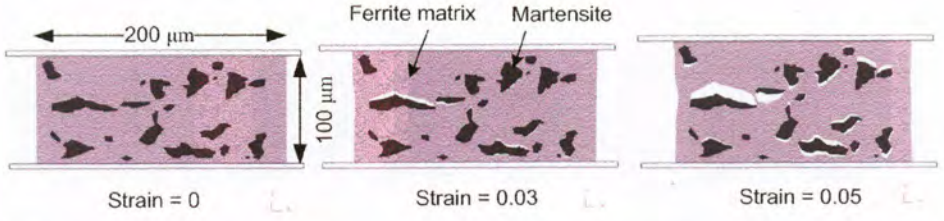

Figure 16. *Evolution of microvoids between martensite and ferrite phases in RVE during deformation*

7. CONCLUSIONS

The following conclusions can be summarized from this study.

- From visual examination of AHSS parts, shear fractures were more often observed in a sharp bending radius, stretch-bending at draw-beads and plane-stain bending areas.
- SEM analyses of fractured sections of a B-pillar part and a draw-bend sample showed similar ductile dimple rupture and a number of micro-voids.
- Stop-tensile tests for DP590 showed the growth and coalescence of micro-voids as the plastic stain increased from UTS to fracture point.
- The micro-void induced damage was emulated by using a damage model with critical damage value (CDV) that was determined from tensile tests and simulations.
- The damage model with CDV showed good agreement with experiments in terms of fracture types (I, II and III) in the draw bend test. However, it underestimated the displacement of front grip at fracture comparing to experiments, while FEM without CDV greatly overestimated it.
- Numerical modeling was conducted to simulate the growth of micro-voids at martensite-ferrite boundaries for real microstructure of DP590. However, it found that the

equilibrium conditions at large strain range were difficult to obtain in simulating the RVE model.

- Therefore, a new damage model based on the area fraction of micro-voids and temperature increase during deformation should be considered to practically implement in process simulations for industry.

8. ACKNOWLEDGEMENTS

This study was conducted with support from the U.S. Department of Energy (Contract DE-FC26-02OR22910), "Failure Analysis of Advanced High Strength Steels (AHSS) During Draw Bending". This support is gratefully acknowledged. The authors thank Dr. James R. Fekete at General Motors Corporation, Dr. Changqing Du at Chrysler LLC, Mr. Mike Bzdok at Auto/Steel Partnership and Dr. Wei-Tsu Wu at Scientific Forming Technologies Corporation (SFTC) for their supports and advices throughout this study.

9. REFERENCES

1. W. Gan, P. H. Zhang, R. H., Wagoner and G. S. Daehn: "Effect of load redistribution in transient plastic flow", Metallurgical and Materials Transactions a-Physical Metallurgy and Materials Science, 37A (2006) 2097-2106
2. K. Hasegawa, K. Kawamura, T. Urabe, and Y. Hosoya: "Effects of microstructure on stretch-flange-formability of 980 MPa grade cold-rolled ultra high strength steel sheets", ISIJ International, 44 (2004) 603-609
3. O. Duber, B. Kunkler, U. Krupp, H.J. Christ, C.P. Fritzen: "Experimental characterization and two-dimensional simulation of short-crack propagation in an austenitic-ferritic duplex steel", International Journal of Fatigue, 28 (2006) 983-992
4. M. Sarwar, E. Ahmad, N. Hussain, B. Ahmad, T. Manzoor: "Crack path morphology in dual-phase steel", Journal of Materials Engineering and Performance, 15 (2006) 352-354
5. M. Sarwar and R. Priestner: "Influence of ferrite-martensite microstructural morphology on tensile properties of dual-phase steel", Journal of Materials Science, 31 (1996) 2091-2095
6. H. Kuwamura and K. Yamamoto: "Ductile crack as trigger of brittle fracture in steel", Journal of Structural Engineering-Asce, 123 (1997) 729-735
7. Z. Marciniak and K. Kuczynski: "Limit strains in the process of stretch forming sheet metal", Int. J. Mech. Sci., 9 (1967) 609–620
8. A. Graf and W. Hosford: "Effect of Changing Strain Paths on Forming Limit Diagrams of Al 2008-T4", Metallurgical Transactions a-Physical Metallurgy and Materials Science, 24 (1993) 2503-2512
9. J. V. Laukonis and A. K. Ghosh: "Effects of strain path changes to the formability of sheet metals", Metallurgical and Materials Transactions a-Physical Metallurgy and Materials Science, 9 (1978) 1849-1856
10. T. B. Stoughton and X. H. Zhu: "Review of theoretical models of the strain-based FLD and their relevance to the stress-based FLD", International Journal of Plasticity, 20 (2004) 1463-1486
11. S. Lee: "Microstructural Influences on the Fracture Behavior of Multi-Phase Sheet Steels", Ph.D. dissertation, Metallurgical and Materials Engineering, Colorado School of Mines, 2005
12. H. Takuda, K. Mori and N. Hatta: "The application of some criteria for ductile fracture to the prediction of the forming limit of sheet metals", Journal of Materials Processing Technology, 95 (1999) 116-121